Localizing spin dynamics in a spin-1 Bose-Einstein condensate via magnetic pulses

Huanbin Li,[1] Zhengguo Pu,[1] M. S. Chapman,[2] and Wenxian Zhang[1,*]
[1]*School of Physics and Technology, Wuhan University, Wuhan, Hubei 430072, China*
[2]*School of Physics, Georgia Institute of Technology, Atlanta, Georgia 30332-0430, USA*
(Received 16 March 2015; published 27 July 2015)

Spin-exchange interaction between atoms in a spin-1 Bose-Einstein condensate causes atomic spin evolving periodically under the single-spatial-mode approximation in the mean-field theory. By applying fast magnetic pulses according to a two-step or a four-step control protocol, we find analytically that the spin dynamics is significantly suppressed for an arbitrary initial state. Numerical calculations under single-mode approximation are carried out to confirm the validity and robustness of these protocols. This localization method can be readily utilized to improve the sensitivity of a magnetometer based on spin-1 Bose-Einstein condensates.

DOI: 10.1103/PhysRevA.92.013630 PACS number(s): 67.85.−d, 03.75.Kk, 03.75.Mn

I. INTRODUCTION

Spin-exchange interaction between atoms in a spin-1 Bose-Einstein condensate (BEC) causes complex spin mixing dynamics and spin diffusion, which is a major obstacle to realize experimentally a high-precision magnetometer based on a spinor BEC [1–8]. In order to improve the sensitivity of the magnetometer, a smaller spin-exchange interaction is required, which may be implemented effectively by the dynamical decoupling method using optical Feshbach resonance techniques [9,10]. In addition, the small spin-exchange interaction can be utilized to resolve the ambiguity of the spin texture in ferromagnetically interacting ^{87}Rb spin-1 BEC, where the spatial texture structure may be induced by the spin-exchange interaction, the magnetic dipolar interaction, or both of them [1,3,11–15].

However, a more experimentalist-friendly proposal to suppress the spin-exchange interaction employs magnetic pulses and microwave pulses, which are much easier to implement and tune experimentally [11,16–20]. By applying a magnetic field to an atomic spin-1 BEC, only the quadratic Zeeman effect δ, which is proportional to the square of the field, is considered because the linear Zeeman effect can be eliminated mathematically by adopting the rotating reference frame due to the conservation of the total magnetization of the spin-1 condensate [2,21,22]. Under current experimental conditions, the effective quadratic Zeeman energy of either the magnetic field or the microwave driving field can be adjusted from -240 Hz to $+240$ Hz, which is about 10 times larger than the spin exchange interaction for typical densities of a ^{87}Rb spin-1 condensate, $\sim 10^{14}$ cm^{-3} [17,18,22].

In this paper, we propose to localize the spin dynamics of a spin-1 BEC by periodically applying magnetic and/or microwave field pulses, which effectively suppress the spin exchange interaction. By applying two-step pulse cycles with only positive δ, the condensate dynamics is localized if the relative phase of the initial state is close to zero; by applying four-step pulse cycles with both positive and negative δ, the condensate dynamics is localized for an *arbitrary* initial state. The exploration of the robustness of the protocols shows that a wide parameter regime exists for a spin-1 condensate under current experimental conditions. This proposal may find its potential application to improve the sensitivity of a practical high-resolution magnetometer based on spin-1 BEC.

This paper is organized as follows. In Sec. II, we review the theoretical description of the free spin mixing dynamics under the single-spatial-mode approximation (SMA) in a spin-1 BEC in a magnetic field, whose quadratic Zeeman splitting δ ranges from large negative values to large positive values. In Sec. III, we analytically design and numerically confirm the control protocols of magnetic and microwave pulses to localize the condensate spin dynamics, where either a two-step or a four-step pulse cycle is employed. Furthermore, the robustness of the control protocols is explored in Sec. IV by assuming 5% random error of the pulse amplitude $\delta(t)$. Finally, a brief summary is presented in Sec. V.

II. FREE SPIN DYNAMICS IN A MAGNETIC FIELD

Within the mean-field theory, the free spin mixing dynamics in a spin-1 BEC with either ferromagnetic or antiferromagnetic spin exchange interaction under the SMA in a magnetic field is described by the following equation of motion [2,9,18]:

$$\begin{aligned}\dot{\rho}_0 &= \frac{2c}{\hbar}\rho_0\sqrt{(1-\rho_0)^2-m^2}\,\sin\theta,\\ \dot{\theta} &= -\frac{2\delta}{\hbar}+\frac{2c}{\hbar}(1-2\rho_0)\\ &\quad+\frac{2c}{\hbar}\,\frac{(1-\rho_0)(1-2\rho_0)-m^2}{\sqrt{(1-\rho_0)^2-m^2}}\cos\theta,\end{aligned}\tag{1}$$

where $c = c_2 N \int d\vec{r}|\phi(\vec{r})|^4$, with N being the total number of atoms in the condensate and $\phi(\vec{r})$ being a normalized spatial mode function under the SMA, which is determined by a scalar Gross-Pitaevskii equation with a spin-independent interaction, $[-(\hbar^2/2M)\nabla^2 + V_{\rm ext}(\vec{r}) + c_0|\phi|^2]\phi(\vec{r}) = \mu\phi(\vec{r})$, where M is the atomic mass and V is the external harmonic trapping potential. The spin-independent coefficient c_0 and spin-exchange coefficient c_2 are given, respectively, by $c_0 = 4\pi\hbar^2(a_0+2a_2)/3M$ and $c_2 = 4\pi\hbar^2(a_2-a_0)/3M$ with the s-wave scattering length a_0 (a_2) for two spin-1 atoms in the compound symmetric channel of total spin 0 (2). For two popular ultracold spin-1 atomic gases in experiments, ^{87}Rb and ^{23}Na, $c_0 \gg |c_2|$ is always satisfied and thus guarantees the validity of the SMA in most experimental situations [22–24].

*Corresponding author: wxzhang@whu.edu.cn

The fractional population of spin component $\rho_\alpha(\alpha = -1,0,+1)$ satisfies $\sum_\alpha \rho_\alpha = 1$. The magnetization $m = \rho_+ - \rho_-$ is constant during the evolution due to the isotropic nature of the spin-exchange interaction. The relative phase among the three components is $\theta = \theta_+ + \theta_- - 2\theta_0$, with θ_α being the phase of the spin wave function. The quadratic Zeeman energy is $\delta = (E_+ + E_- - 2E_0)/2$, with E_α being the Zeeman energy shift of the component. In general, $\delta \approx 72B^2$ Hz/G^2 for ^{87}Rb BECs and $\delta \approx 278B^2$ Hz/G^2 for ^{23}Na BECs, where the magnetic field B is in units of Gauss. Due to the conservation of the magnetization m, the linear Zeeman energy $(E_- - E_+)/2$ can be eliminated mathematically by adopting a rotating reference frame.

The total spin energy is constant during the free evolution of the spin-1 condensate in a magnetic field,

$$\varepsilon = c\rho_0[(1-\rho_0) + \sqrt{(1-\rho_0)^2 - m^2}\cos(\theta)] + \delta(1-\rho_0).$$

Starting from a given initial state, which is usually a ground state in a magnetic field in experiments, the condensate evolves according to an isoenergy trajectory in the plane of ρ_0-θ by abruptly changing the magnetic field to a different value. By taking into account the energy conservation, Eq. (1) is further simplified as $(\dot{\rho_0})^2 = (4/\hbar^2)\{[\varepsilon - \delta(1-\rho_0)][(2c\rho_0 + \delta)(1-\rho_0) - \varepsilon] - (c\rho_0 m)^2\}$; thus, the time evolution of ρ_0 can be analytically expressed in terms of the Jacobian elliptic function $cn(\cdot,\cdot)$ if $\delta \neq 0$ and the sinusoidal function if $\delta = 0$ [2,9,25],

$$\rho_0(t) = \tfrac{1}{2}[x_2 + x_1 - (x_2 - x_1)\sin(\gamma_0 + 2t\sqrt{2c\varepsilon + c^2m^2})] \tag{2}$$

for $\delta = 0$;

$$\rho_0(t) = x_2 + (x_3 - x_2)cn^2[\gamma_0 + t\sqrt{2c\delta(x_3 - x_1)}, k] \tag{3}$$

for $c\delta > 0$;

$$\rho_0(t) = x_2 - (x_2 - x_1)cn^2[\gamma_0 + t\sqrt{-2c\delta(x_3 - x_1)}, k] \tag{4}$$

for $c\delta < 0$. We have set $\hbar = 1$. Here $x_1 \leqslant x_2 \leqslant x_3$ ($x_1 \leqslant x_2$ for $\delta = 0$) are the roots of $\dot{\rho_0} = 0$, $k = \sqrt{(x_3 - x_2)/(x_3 - x_1)}$ if $c\delta > 0$, and $k = \sqrt{(x_2 - x_1)/(x_3 - x_1)}$ if $c\delta < 0$. γ_0 is determined by the initial state [i.e., $\sin(\gamma_0) = (x_1 + x_2 - 2\rho_{0i})/(x_2 - x_1)$ for $\delta = 0$]. Hereafter we assume $c = -1$; thus, the energy unit is $|c|$, the time unit is $|c|^{-1}$, and $m = 0$.

Typical trajectories are illustrated in Fig. 1(a) for different δ. Although starting from the same initial state, the trajectories could cover the whole ρ_0-θ plane if the quadratic Zeeman energy δ is continuously varied from negative infinity to positive infinity. All the trajectories are classified into two modes: the oscillatory mode where θ is in the range $[-\pi,\pi]$ and the running phase mode where θ goes beyond $[-\pi,\pi]$. As shown clearly in Fig. 1(a), the oscillatory mode trajectories evolve in a clockwise (counterclockwise) direction if $c < 0$ ($c > 0$), while the running phase mode trajectories for large $|\delta| \gg |c|$ may take one of two opposite directions, depending on the sign of δ. This is a key point in order to localize the condensate spin dynamics. The boundaries between the oscillatory modes and the running phase modes satisfy one of the two requirements, $\rho_0(t) = 0$ ($\delta = \delta_-$) or 1 ($\delta = \delta_+$) if time is long. The corresponding period T becomes infinite [see also Fig. 1(b)]. Another special point $\delta = \delta_0$ denotes the coincidence of the initial state with the ground state; thus, the oscillation amplitude A is zero, but the period T is finite.

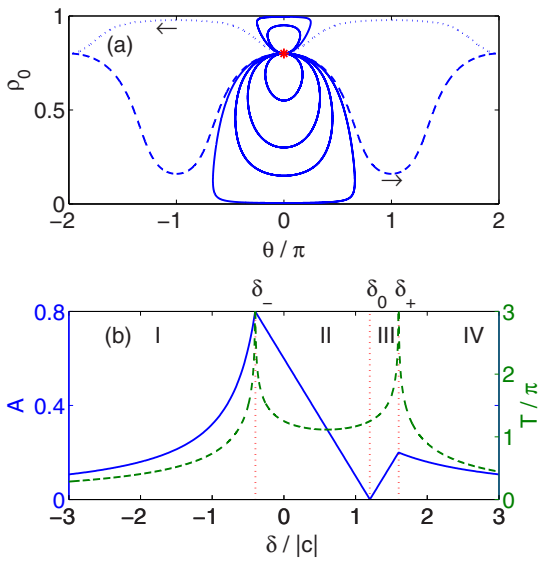

FIG. 1. (Color online) (a) Typical trajectories in the ρ_0-θ plane for $\delta/|c| = -0.5$ (dashed line), -0.39, $-0.1,0.2,0.7,1.5,1.59$ (solid lines), and 1.8 (dotted line), from bottom to top. All the trajectories with solid lines evolve in a clockwise direction. The initial state (asterisk) is $\rho_0(0) = \rho_{0i} = 0.8$ and $\theta(0) = \theta_i = 0$. (b) Dependence of the oscillation amplitude A (blue solid line) and the period T (green dashed line) of ρ_0 on δ. The running phase modes correspond to regions I and IV, and the oscillatory modes correspond to regions II and III. The red dotted lines marked by δ_0 and $\delta_\pm$ denote, respectively, the ground-state quadratic Zeeman energy (the initial state coincides with the ground state and A is zero) and the resonant quadratic Zeeman energy (T is infinite and $\rho_0 \to 0$ or 1).

The oscillation amplitudes and the periods are shown in Fig. 1(b). There are clearly four regions: (I) a running phase mode with increasing $\theta(t)$, (II) an oscillatory mode with $0 < \rho_0(t) \leqslant \rho_{0i}$, (III) an oscillatory mode with $\rho_{0i} < \rho_0(t) < 1$, and (IV) a running phase mode with decreasing $\theta(t)$. The amplitude of the oscillations A monotonically increases in regions I and III but decreases in regions II and IV with increasing δ. The period of the oscillations T shows two resonant peaks at $\delta = \delta_\pm$, where $\rho_0(t) = 0$ or 1 at long enough time. The period is almost a constant between these two peaks but decreases rapidly outside the peaks. Similar oscillation behaviors were also observed in antiferromagnetically interacting ^{23}Na spin-1 condensates ($c > 0$) [18,19].

We observe from Fig. 1(a) that in the oscillatory mode θ increase or decrease with time if $\theta \approx 0$ and ρ_0 is around its extremes. We may utilize this property to localize the condensate dynamics around $\theta \approx 0$ by canceling θ in a period with θ increasing (decreasing) during the first (second) part. For an arbitrary state, however, we may utilize both the oscillatory and the running phase modes to localize the dynamics since θ may increase or decrease for a given ρ_0, depending on the value of δ.

III. LOCALIZED SPIN DYNAMICS

We consider first that the control period consists of two steps, a free evolution ($\delta = 0$) for a time slot τ_1, which

guarantees $\rho_0(\tau_1) = \rho_{0i}$ and $\theta(\tau_1) = -\theta_i$, followed by an evolution in a magnetic field $\delta = d$ for a time slot τ_2, which guarantees $\rho_0(\tau_1 + \tau_2) = \rho_{0i}$ and $\theta(\tau_1 + \tau_2) = \theta_i$. We hereafter refer to this protocol as the two-step control. For a given initial state with $\theta_i \approx 0$, it is easy to prove analytically that τ_1 depends on the initial state and τ_2 depends uniquely on d, which indicates that there is only one free parameter in the two-step control protocol. The time dependence of the magnetic field for the two-step control is

$$\delta(t) = \begin{cases} 0, & j(\tau_1+\tau_2) \leqslant t < j(\tau_1+\tau_2)+\tau_1, \\ d, & j(\tau_1+\tau_2)+\tau_1 \leqslant t < (j+1)(\tau_1+\tau_2), \end{cases}$$

where $j = 0,1,2,\ldots$ is an integer denoting the number of control cycles.

Typical controlled trajectories are illustrated in Fig. 2(a) for three values of d, where the initial state is $\rho_{0i} = 0.8$ and $\theta_i = -0.1\pi$ [26]. We see clearly that the oscillations of both ρ_0 and θ under the two-step control are smaller than that during free evolution, indicating that the condensate dynamics is indeed localized by the two-step control protocol. Starting from the same initial state, the lager d is, the smaller the oscillation of ρ_0 is.

The condensate spin average is $\langle \boldsymbol{F} \rangle = \langle F_x \rangle \hat{x} + \langle F_y \rangle \hat{y} + \langle F_z \rangle \hat{z}$ for a state with [2]

$$\langle F_x \rangle + i \langle F_y \rangle = 2\sqrt{\rho_0(1-\rho_0)}\cos(\theta/2),$$
$$\langle F_z \rangle = 0.$$

Once we localize $\rho_0(t)$ and $\theta(t)$, the condensate spin $\langle \boldsymbol{F} \rangle$ is obviously localized. For a nonzero $\langle F_z \rangle$, the localization occurs similarly.

The cycle period T depends on the free evolution time τ_1 and the controlled evolution time τ_2. The free evolution time

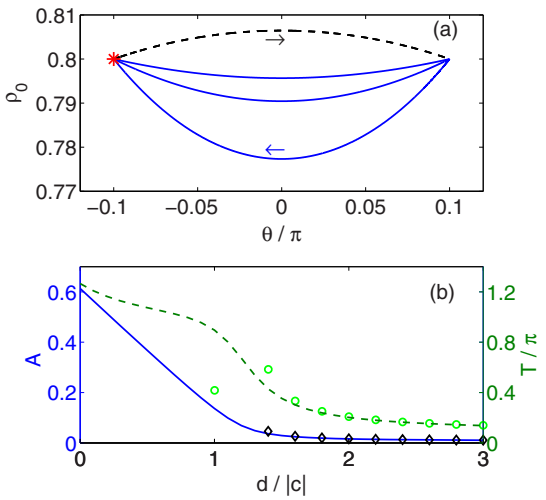

FIG. 2. (Color online) (a) Typical trajectories under the modulation of $\delta(t)$. Each modulation cycle includes a free evolution with $\delta = 0$ (dashed line) and a controlled evolution with $d/|c| = 1.5,2.0,3.0$ (solid lines, from bottom to top). The initial state (red asterisk) is $\rho_{0i} = 0.8$ and $\theta_i = -0.1\pi$. (b) Dependence of the amplitude (blue solid line) and period (green dashed line) of ρ_0 on d, the nonzero quadratic Zeeman splitting. Circles and diamonds are the period and amplitude calculated analytically with Eqs. (7) and (8) for large d's, respectively.

is determined by the evolution time of the system from its initial state ρ_{0i} and θ_i to the symmetric state $\rho_0(\tau_1) = \rho_{0i}$ and $\theta(\tau_1) = -\theta_i$. In this way, the time τ_1 is calculated analytically by using Eq. (2),

$$\tau_1 = (\pi/2 - \gamma_0)/\sqrt{2c\,\varepsilon + c^2 m^2}, \tag{5}$$

and γ_0 is calculated by using Eq. (2), $\sin(\gamma_0) = (x_1 + x_2 - 2\rho_{0i})/(x_2 - x_1)$. In the limit of small $\theta \ll 1$, $\tau_1 \approx |\theta_i/[2c(1-2\rho_{0i})]|$, where we have used $\rho_0(t) \approx \rho_{0i}$. Similarly, the controlled evolution time τ_2 is the evolution time of the system in the magnetic field $\delta = d$ and can be calculated by using the conditions $\rho_0(T) = \rho_{0i}$ and $\theta(T) = \theta_i$,

$$\tau_2 = \sqrt{2}\gamma_0'/\sqrt{-c\,d(x_3 - x_1)}, \tag{6}$$

and γ_0' is calculated by using Eq. (3), $cn^2(\gamma_0',k) = (\rho_{0i} - x_2)/(x_3 - x_2)$. In the limit of small $\theta \ll 1$ and large d, $\tau_2 \approx |\theta_i/[2c(1-2\rho_{0i}) - d]|$. In total, the cycle period is approximated as

$$T \approx \left| \frac{\theta_i\, d}{2c(1-2\rho_{0i})[2c(1-2\rho_{0i}) - d]} \right| \tag{7}$$

for small θ_i and large d. We notice that $T \approx \tau_1$ for large d, as shown in Fig. 2(b).

We define the control oscillation amplitude as $A = \max(\rho_0) - \min(\rho_0)$, which depends obviously on the initial state and the magnetic field d. The amplitude can be calculated analytically but is too lengthy to present here. In the limit of large d and small θ_i, the amplitude is approximately

$$A = A_1 + A_2, \tag{8}$$

where

$$A_1 \approx \frac{\rho_{0i}(1-\rho_{0i})}{4(2\rho_{0i}-1)}\,\theta_i^2, \quad A_2 \approx \frac{\rho_{0i}(1-\rho_{0i})}{|2d/c| - 4(2\rho_{0i}-1)}\,\theta_i^2.$$

We see that A approaches A_1 as d goes to infinity.

In Fig 2(b), we present the dependence of A and T on the control magnetic field d. We see clearly that A and T decrease monotonically as d increases, manifesting the fact that better localization of the condensate dynamics is achieved in a higher magnetic field. We note that A and T approach their *nonzero* asymptotic values at large values of d. Actually, to reduce the oscillation amplitude A further down to zero, we have to employ the following four-step control protocol.

We consider next that the control period consists of four steps, (i) a free evolution for a time τ_1, (ii) an evolution in a magnetic field with $\delta = d_1$ for a time τ_2, (iii) a second free evolution for the time τ_3, and (iv) a second controlled evolution in another magnetic field with $\delta = d_2$ for a time τ_4, as shown in Fig. 3(a). We refer to this protocol as the four-step control. For simplicity but without loss of generality, we limit ourselves to the symmetric situations where $d_1 = -d_2 = d$ and $\tau_3 = \tau_1 = \tau$. It will be analytically proved that τ_2 and τ_4 are uniquely determined by d and τ. Thus, there are only two free parameters, d and τ, in the four-step control we considered here.

It is straightforward to find the analytical solution to τ_2 and τ_4 by using the initial state and Eqs. (2)–(4),

$$\tau_2 = \frac{\sqrt{2}\gamma_0}{\sqrt{-cd(x_3 - x_1)}}, \quad \tau_4 = \frac{\sqrt{2}\gamma_0'}{\sqrt{cd(x_3' - x_1')}};$$

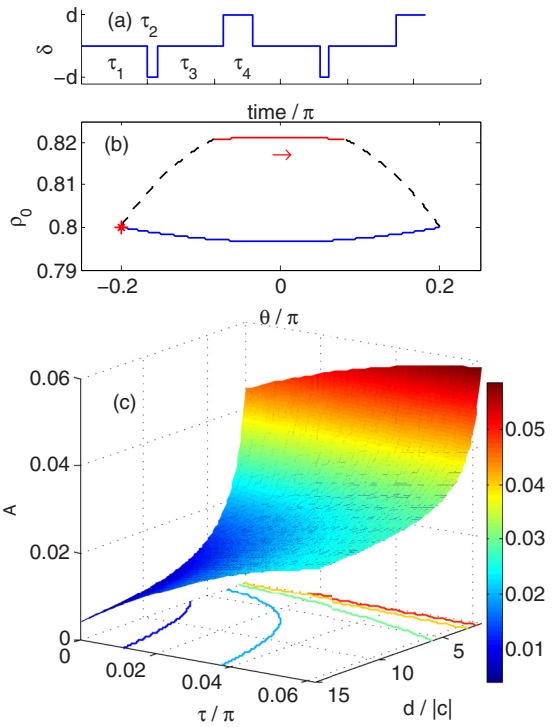

FIG. 3. (Color online) (a) Schematic of a magnetic pulse sequence. (b) Typical controlled trajectory of $\rho_0(t)$ and $\theta(t)$ under a four-step pulse sequence of $\delta(t)$ for a four-step protocol. The red asterisk marks the initial state. The parameters are $\rho_{0i} = 0.8$, $\theta_i = -0.2\pi$, $d/|c| = 10$, and $\tau_1 = \tau_3 = \tau = 0.05\pi$. The values of τ_2 and τ_4 are calculated, $\tau_2 \approx 0.0072\pi$ and $\tau_4 \approx 0.0226\pi$. (c) Amplitude of ρ_0 under four-step pulse sequences. Better localization of ρ_0 (smaller A) is achieved for larger d and smaller τ.

γ_0' and $x_{3,1}'$ are determined by $\rho_0(\tau)$ and $-\theta(\tau)$. We note here that the initial state for τ_2 is $\rho_0(\tau)$ and $\theta(\tau)$, and that for τ_4 is ρ_{0i} and $-\theta_i$. The total period for a complete cycle is

$$T = 2\tau + \frac{\sqrt{2}\gamma_0}{\sqrt{-cd(x_3 - x_1)}} + \frac{\sqrt{2}\gamma_0'}{\sqrt{cd(x_3' - x_1')}}. \quad (9)$$

Typical controlled evolution of the condensate is illustrated in Fig. 3(b), where the parameters are given in the caption. Compared to the two-step control protocol, there are two advantages. The first is that the initial state is arbitrary; particularly, θ_i goes beyond the smallness requirement. The second is that the oscillation amplitude and period approach zero if d is large enough and τ is short enough, as shown in Fig. 3(c) and Eq. (9).

IV. ROBUSTNESS OF THE CONTROL PROTOCOLS

We have assumed the magnetic control pulses are perfect in the previous sections, but there are always uncontrollable errors in practical experiments; for example, the microwave field δ [18] and the initial θ_i may have relative uncertainty. Since the timing is pretty accurate in current experiments, we next evaluate the robustness of the two-step and four-step protocols under only 5% uncertainty of δ or θ_i for many control cycles.

We define the fidelity of a protocol after many control cycles as

$$F = |\langle\vec{\xi}_i|\vec{\xi}_f\rangle|^2, \quad (10)$$

where $|\vec{\xi}_{i,f}\rangle$ is the initial and the final state of the spin-1 condensate and satisfies $|\langle\vec{\xi}|\vec{\xi}\rangle|^2 = 1$. The state has three components, $|\vec{\xi}\rangle = (\xi_+, \xi_0, \xi_-)^T$, with $\xi_\alpha = \sqrt{\rho_\alpha}e^{-i\theta_\alpha}$ ($\alpha = -1, 0, +1$) and ρ_α and θ_α being the fraction and the phase of component α, respectively. The fidelity measures how close the initial and the final states are. The fidelity is 1 for ideal pulses but lower than 1 in the presence of pulse errors. The larger the errors are, the lower the fidelity is. Higher fidelity indicates more robustness of the protocol to errors.

We assume the magnetic-field error is distributed with equal probability in the range $[0.95, 1.05]d$ with an average of d. For the four-step protocols, the errors for d_1 and d_2 ($|d_1| = |d_2| = d$) are independent. We numerically calculate the dependence of the fidelity F on d. The initial state is $\rho_{0i} = 0.8$, $\theta_i = -0.1\pi$ for two-step protocols and $\rho_{0i} = 0.8$, $\theta_i = -0.2\pi$ for four-step protocols.

The results are shown in Fig. 4(a) for two-step protocols and in Fig. 4(b) for four-step protocols with an error of δ.

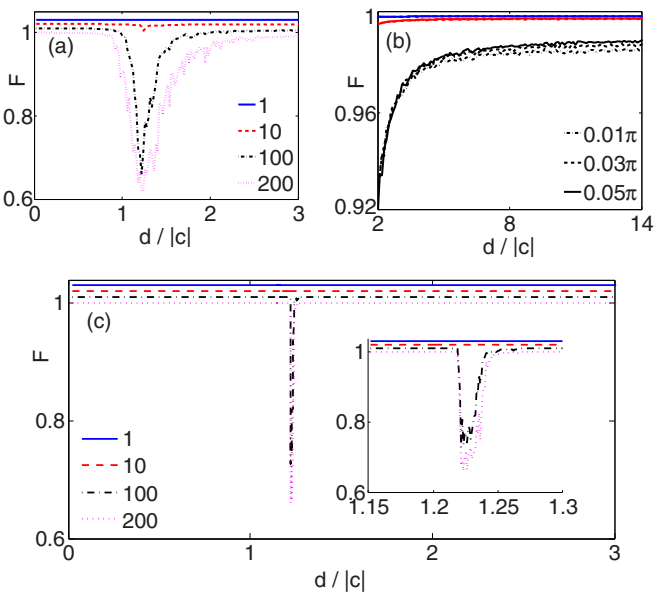

FIG. 4. (Color online) (a) Fidelity after 1 cycle (blue solid line), 10 cycles (red dashed line), 100 cycles (black dash-dotted line), and 200 cycles (purple dotted line) for the two-step protocol with 5% relative uncertainty in δ. For clarity, each curve is shifted up by 0.01 from bottom to top. (b) Fidelity after 1 cycle [blue (dark gray) solid line], 10 cycles [red (light ray) solid line], and 100 cycles (black lines) while $\tau/\pi = 0.01$ (dash-dotted line), 0.03 (dashed line), and 0.05 (solid lines) for the four-step protocol with 5% relative uncertainty in δ. (c) Fidelity after 1 cycle (blue solid line), 10 cycles (red dashed line), 100 cycles (black dash-dotted line), and 200 cycles (purple dotted line) for the two-step protocol with 5% relative uncertainty in θ_i. Each curve is also shifted up by 0.01 from bottom to top. The inset shows a zoom-in view near the dip in the main panel. The results show that both the two-step protocol and the four-step protocol are robust against errors.

As shown in Fig. 4(a), the fidelity, which is, after a few cycles, under the uncertainty of δ, is above 99% for most d, except a sharp dip near $d/|c| \approx 1.2$. This dip is nothing but $d = \delta_0$ where the period T is most sensitive to the change of d [i.e., the largest derivative of T with respect to d in Fig. 2(b)]. The dip becomes wider and deeper after more cycles. Clearly, the two-step protocol is robust except when $d \approx \delta_0$. For the four-step protocol, as shown in Fig. 4(b), we find that the fidelity is very close to 1, particularly for large d's, although it decreases as τ decreases after many cycles under the uncertainty of δ. By taking into account the requirements of small τ and large d to better localize the condensate dynamics [see Fig. 3(c)], both requirements on the localization and the robustness can be satisfied simultaneously in practical experiments.

For the errors in the initial relative phase, we also assume an equal distribution probability in the range $[0.95, 1.05]\theta_i$ with an average of θ_i. In Fig. 4(c), the fidelity is again very close to 1 except a sharp dip around $d/|c| = \delta_0$, similar to Fig. 4(a). This result shows that the two-step control protocol is pretty robust under the uncertainty of θ_i if we choose a field away from the dip. Strikingly, the fidelity for the four-step protocol with the error of θ_i is always above 99.99% within 100 cycles, showing the superrobustness of the protocol against this kind of error.

V. CONCLUSION

We propose to localize the spin mixing dynamics in a spin-1 Bose condensate by periodically applying magnetic pulse sequences, according to the two-step protocol for an initial state with a small initial relative phase or the four-step protocol for an arbitrary initial state. Numerical calculations confirm the validity of the proposal for a ferromagnetically interacting spin-1 condensate under the single-spatial-mode approximation. We further illustrate the robustness of the localization protocol with numerical calculations by assuming 5% uncertainty of the magnetic pulse amplitude and θ_i, which might occur in practical experiments [18]. Our proposal may be utilized to realize higher-precision magnetometers based on spinor BEC [4,27] or to explore the weak dipolar interaction effects in ^{87}Rb spin-1 condensates by suppressing the spin dynamics induced by the spin-exchange interaction [3,11,15,28,29].

ACKNOWLEDGMENTS

This work is supported by National Basic Research Program of China Grant No. 2013CB922003, National Natural Science Foundation of China Grant No. 11275139, National Science Foundation (US) Grant No. 1208828, and the Fundamental Research Funds for the Central Universities.

[1] M. Chang, Q. Qin, W. Zhang, L. You, and M. Chapman, Nat. Phys. **1**, 111 (2005).
[2] W. Zhang, D. L. Zhou, M.-S. Chang, M. S. Chapman, and L. You, Phys. Rev. A **72**, 013602 (2005).
[3] L. E. Sadler, J. M. Higbie, S. R. Leslie, M. Vengalattore, and D. M. Stamper-Kurn, Nature (London) **443**, 312 (2006).
[4] M. Vengalattore, J. M. Higbie, S. R. Leslie, J. Guzman, L. E. Sadler, and D. M. Stamper-Kurn, Phys. Rev. Lett. **98**, 200801 (2007).
[5] F. K. Abdullaev, J. G. Caputo, R. A. Kraenkel, and B. A. Malomed, Phys. Rev. A **67**, 013605 (2003).
[6] Y. Liu, S. Jung, S. E. Maxwell, L. D. Turner, E. Tiesinga, and P. D. Lett, Phys. Rev. Lett. **102**, 125301 (2009).
[7] S. K. Steinke, S. Singh, P. Meystre, K. C. Schwab, and M. Vengalattore, Phys. Rev. A **88**, 063809 (2013).
[8] D. M. Stamper-Kurn and M. Ueda, Rev. Mod. Phys. **85**, 1191 (2013).
[9] W. Zhang, B. Sun, M. S. Chapman, and L. You, Phys. Rev. A **81**, 033602 (2010).
[10] B.-Y. Ning, J. Zhuang, J. Q. You, and W. Zhang, Phys. Rev. A **84**, 013606 (2011).
[11] M. Vengalattore, S. R. Leslie, J. Guzman, and D. M. Stamper-Kurn, Phys. Rev. Lett. **100**, 170403 (2008).
[12] M. Vengalattore, J. Guzman, S. R. Leslie, F. Serwane, and D. M. Stamper-Kurn, Phys. Rev. A **81**, 053612 (2010).
[13] Y. Kawaguchi, H. Saito, K. Kudo, and M. Ueda, Phys. Rev. A **82**, 043627 (2010).
[14] B.-Y. Ning, S. Yi, J. Zhuang, J. Q. You, and W. Zhang, Phys. Rev. A **85**, 053646 (2012).
[15] Y. Eto, H. Saito, and T. Hirano, Phys. Rev. Lett. **112**, 185301 (2014).
[16] F. Gerbier, A. Widera, S. Fölling, O. Mandel, and I. Bloch, Phys. Rev. A **73**, 041602 (2006).
[17] T. M. Hoang, C. S. Gerving, B. J. Land, M. Anquez, C. D. Hamley, and M. S. Chapman, Phys. Rev. Lett. **111**, 090403 (2013).
[18] L. Zhao, J. Jiang, T. Tang, M. Webb, and Y. Liu, Phys. Rev. A **89**, 023608 (2014).
[19] J. Jiang, L. Zhao, M. Webb, and Y. Liu, Phys. Rev. A **90**, 023610 (2014).
[20] Y. Eto, M. Sadgrove, S. Hasegawa, H. Saito, and T. Hirano, Phys. Rev. A **90**, 013626 (2014).
[21] J. Stenger, S. Inouye, D. M. Stamper-Kurn, H.-J. Miesner, A. P. Chikkatur, and W. Ketterle, Nature (London) **396**, 345 (1998).
[22] W. Zhang, S. Yi, and L. You, New J. Phys. **5**, 77 (2003).
[23] C. K. Law, H. Pu, and N. P. Bigelow, Phys. Rev. Lett. **81**, 5257 (1998).
[24] S. Yi, O. E. Müstecaplıoğlu, C. P. Sun, and L. You, Phys. Rev. A **66**, 011601(R) (2002).
[25] H. Pu, C. K. Law, S. Raghavan, J. H. Eberly, and N. P. Bigelow, Phys. Rev. A **60**, 1463 (1999).
[26] The initial state in Fig. 2(a) may be realized in experiment by starting from a ground state of a spin-1 BEC in a certain magnetic field, where $\rho_0 = x_2$ and $\theta = 0$. Then we turn off the magnetic field and let the condensate evolve freely for a time period $\tau_1/2$. The initial state is reached after another evolution for a period τ_2 in the control magnetic field d.
[27] Y. Eto, H. Ikeda, H. Suzuki, S. Hasegawa, Y. Tomiyama, S. Sekine, M. Sadgrove, and T. Hirano, Phys. Rev. A **88**, 031602 (2013).
[28] Y. Kawaguchi, H. Saito, and M. Ueda, Phys. Rev. Lett. **98**, 110406 (2007).
[29] W. Zhang, S. Yi, M. S. Chapman, and J.-Q. You (unpublished).